Catalytic diesel particulate filters with highly dispersed ceria: Effect of the soot-catalyst contact on the regeneration performance

Valeria Di Sarli [a,*], Gianluca Landi [a], Luciana Lisi [a], Anna Saliva [b], Almerinda Di Benedetto [b]

[a] Istituto di Ricerche sulla Combustione, Consiglio Nazionale delle Ricerche (CNR), Piazzale V. Tecchio 80, 80125 Napoli, Italy
[b] Dipartimento di Ingegneria Chimica, dei Materiali e della Produzione Industriale, Università degli Studi di Napoli Federico II, Piazzale V. Tecchio 80, 80125 Napoli, Italy

ARTICLE INFO

ABSTRACT

In this work, the effect of the soot-catalyst contact on the regeneration performance of a diesel particulate filter (DPF) wash-coated with nano-metric ceria particles was investigated. The catalyst load was suitably chosen to avoid major changes in pore size distribution of the original filter. Different amounts of soot were loaded into the filter, thus varying the catalyst/soot ratio. Filter samples were characterized by N_2 physisorption at 77 K, Hg intrusion porosimetry and SEM/EDX analysis. Regeneration tests were performed in a lab-scale plant by temperature programmed combustion of soot.

At the lowest soot load explored (corresponding to catalyst/soot ratio ∼100 w/w), the soot particles deeply penetrate into the macro-pores of the filter walls coming in close touch with highly dispersed ceria. At the highest soot load explored (catalyst/soot ratio ∼20 w/w), in addition to the soot particles trapped inside the macro-pores, a thick soot cake layer accumulates on top of the catalytic walls of the filter. The former condition results in a large fraction of soot burned via catalytic path (around 80%—almost purely catalytic regeneration mode) and, thus, in good regeneration performance (e.g., temperature at which 10% of the initial soot is converted, $T_{10\%}$, equal to around 350 °C). Conversely, due to the poor cake-catalyst contact, the latter condition results in a large fraction of soot burned via thermal path (around 80%—catalyst-assisted thermal regeneration mode) and, thus, in much worse regeneration performance (e.g., $T_{10\%}$ ∼475 °C).

This study highlights the importance of strategies that avoid or minimize the segregation between the cake layer and the catalytic wall of the filter to operate catalyst-coated DPFs in an effective manner.

© 2016 Elsevier B.V. All rights reserved.

1. Introduction

Catalytic regeneration of diesel particulate filters (DPFs) has been proposed as an alternative or complementary approach to bypass or mitigate the drawbacks associated with thermal regeneration (additional energy costs, complex means of control, local temperature excursions sufficiently high to damage the DPF, etc.) [1–3]. In principle, the catalyst may be used to achieve soot oxidation at temperatures lower (250–550 °C) than those required for thermal regeneration (>600 °C), and/or to shorten the regeneration time period, thus allowing for energy saving.

From the filtration point of view, the main problem of catalytic (i.e., catalyst-coated) DPFs (CDPFs) is the increase in pressure drop as compared to the bare filter, due to the additional resistance to the gas flow opposed by the wash-coat layer located on top of the porous wall of the filter [4]. However, this problem can be overcome and, thus, the filtration properties preserved, utilizing the porous wall of the DPF substrate, with its large total volume, as support for a thin catalytic layer without causing major changes in pore size distribution [5]. Techniques as sol-gel synthesis have been proposed for filter coating to enable low pressure drop [6].

From the regeneration point of view, there is still no general consensus regarding the ability of CDPFs to oxidize soot at low temperatures and under conditions relevant to practical applications [7]. Indeed, such ability is strictly dependent not only on the intrinsic catalyst activity, but also on the efficiency of the contact between the soot particles and the active sites of the catalyst particles [8,9].

Ceria (alone or in combination with other oxides) is among the most active catalysts for soot oxidation due to its redox properties (Ce^{4+}/Ce^{3+}) and oxygen storage capacity [10,11]. Furthermore, the low cost (as compared to noble metals) makes ceria-based materials particularly attractive.
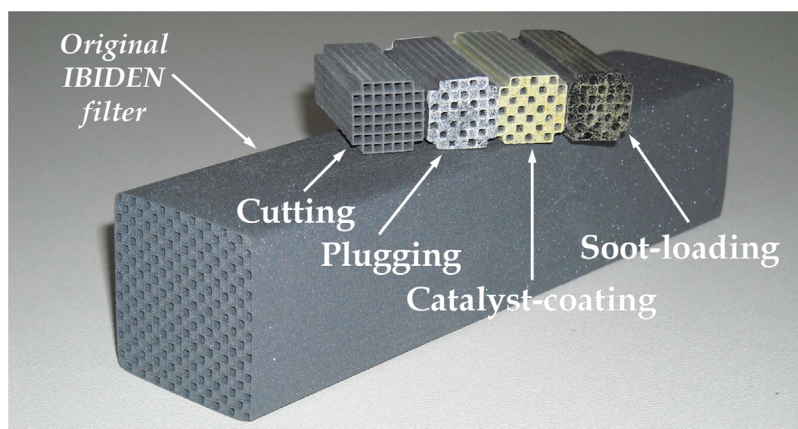
Fig. 1. Monoliths after the steps of cutting, plugging, catalyst-coating and soot-loading (the original IBIDEN filter is also shown).
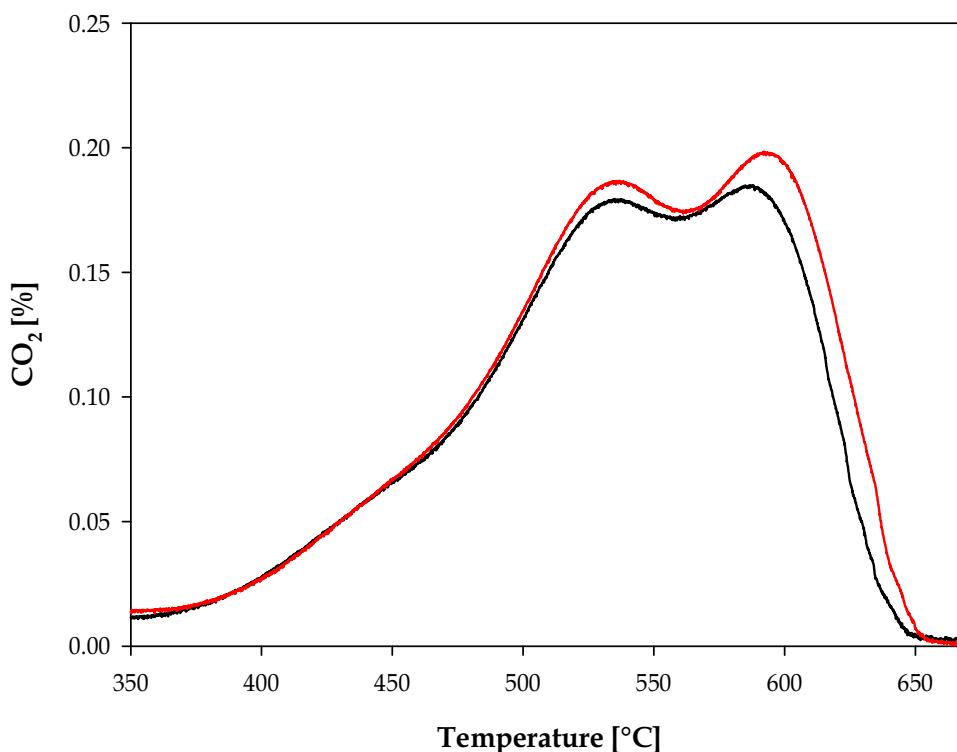

Fig. 2. CO_2 concentration-filter temperature profiles as measured during two independent regeneration tests carried out on filters with catalyst/soot ratio equal to 45 w/w.

Two mechanisms of ceria-catalyzed soot combustion have been identified: the so-called "active oxygen" mechanism and the "NO_2-assisted" mechanism [11]. These two mechanisms may occur simultaneously in soot/O_2/NO reaction.

In the "active oxygen" mechanism, the exchange of oxygen atoms between the ceria catalyst and the O-containing gases (O_2 is the most abundant one in a diesel exhaust) produces highly reactive oxygen species at the catalyst surface (the so-called "active oxygen"), which can oxidize soot very efficiently. However, active oxygen species must be transferred from the ceria catalyst to the soot particles (i.e., to the soot-catalyst interface), before they recombine with each other to form O_2. This transfer process, which occurs by superficial diffusion, makes the soot-ceria contact a key issue for an efficient soot combustion. Once surface oxygen-carbon complexes are formed upon O_2 oxidation, they decompose and yield CO/CO_2, whereas the free carbon sites created on the surface become available to chemisorb further oxidizing molecules.

In the "NO_2-assisted" mechanism, the ceria catalyst catalyzes NO oxidization to NO_2, which is more reactive than O_2 and, as such, can initiate soot combustion. Once NO_2 reacts with soot, the remaining part of the mechanism is similar to that described for "active oxygen".

In order to increase the number of soot-catalyst contact points, thus favoring the solid–solid interaction, ceria-based catalysts with engineered morphologies, such as fibers, sticks, flakes, cubes, rods and stars, have been proposed [4,12–16]. Bensaid et al. [12] compared fibers, sticks and flakes, showing that the fibrous morphology is the best one for soot oxidation, probably due to the network of fibers which surround the soot particles, thus maximizing the number of contact points. On the other hand, the self-assembled stars synthetized by Miceli et al. [15], so-called due to their branched morphology characterized by individual rods assembled in three-dimensional star-shaped way starting from a central nucleus, also exhibit a high availability of contact points between the soot par-
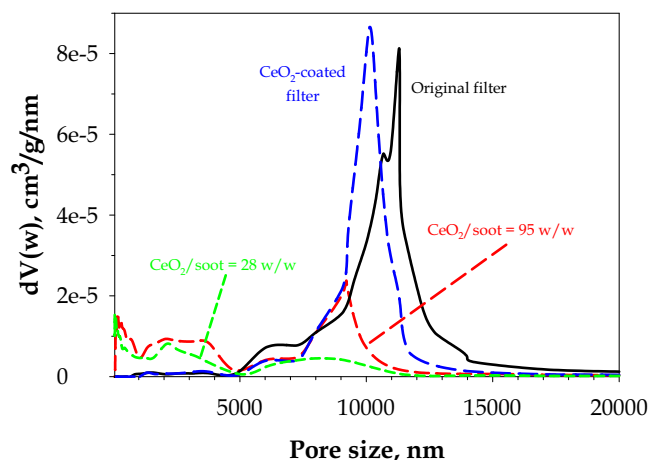
Fig. 3. Pore size distribution (PSD) in the region of macro-pores for original filter, CeO_2-coated filter and two filters with different CeO_2/soot ratios.

ticles and the catalyst itself, each rod offering a concave space for soot intrusion.

All the proposed engineered morphologies have been successfully tested in powdered soot-catalyst mixtures and, thus, under conditions of soot-catalyst contact that, even in the case of the "loose" contact conditions (e.g., soot and catalyst mixed with a spatula), which are more realistic testing conditions than the "tight" contact ones (e.g., soot and catalyst mixed in a mortar) [8], are quite far from those actually established during filter regeneration.

In CDPFs, two zones may be conceptually distinguished: an internal zone and an external zone. The internal zone is the catalytic porous wall of the filter, the external one is the cake layer accumulated onto the porous filter surface. Yapaulo et al. [17] carried out a detailed analysis on the fate of soot in real filters. Their results have shown that, although some soot deeply penetrates into the wall, the majority of soot stays very close to the wall. Thus, a good contact can be established between the soot trapped inside the wall and the catalyst. Conversely, the contact between the cake layer and the catalyst remains limited due to the low surface area available to the interaction between the two solid phases. As a consequence, results of studies on optimal soot-catalyst contact performed on powdered soot-catalyst mixtures can be extrapolated only to the internal zone, the external one being somewhat segregated from the catalyst [9,18].

To mimic the soot-catalyst contact achieved inside a real filter, Rico Pérez and Bueno-López [19] loaded an optimized ceria-praseodymia active phase on DPFs, and designed an experimental set-up where a suspension of soot particles in air is forced to pass through the filter, simulating the filtering process in a real exhaust pipe. Results of regeneration tests performed at different soot loads (while keeping constant the catalyst load) have allowed the identification of a critical catalyst/soot ratio below which the catalytic regeneration is hindered. This has been attributed to the weakening of the soot-catalyst contact. However, the link between the critical ratio and the distribution of soot inside and on top of the catalytic porous wall of the filter has not been quantified.

The present paper fits in this framework with the aim at gaining insight into the role played by both external and internal zones in affecting the regeneration performance of CDPFs. To this end, filters cut from commercial silicon carbide (SiC) DPFs and washcoated with (the same amount of) nano-metric ceria were loaded with different amounts of soot, thus varying the catalyst/soot ratio. Filter samples were characterized by N_2 physisorption at 77 K, Hg intrusion porosimetry and SEM/EDX analysis, to study the modification in pore structure and morphology of the original commercial

filter upon CeO_2 coating and/or soot deposition. Regeneration tests were performed in a lab-scale plant by temperature programmed combustion of soot under an O_2/N_2 atmosphere. Thus, the role of ceria in this study is to catalyze direct combustion of the soot particles trapped inside the filter and not to catalyze NO oxidization to NO_2.

2. Materials and methods

2.1. Filter preparation

The filters were obtained starting from a commercial silicon carbide (SiC) filter (IBIDEN - 180 cpsi; porosity = 0.42) cut in the desired shape and size (cylinder; D = 1.3 cm; L = 3 cm). Due to the loss of the original plugs, a ceramic paste (Rescor Castable Ceramics, 770, COTRONICS CORP.) was used to plug the opposite ends of adjacent channels of the monolith (thus recovering the original filter configuration). In order to harden the plugs, the filters were left at room temperature for about 24 h and, then, calcined at 950 °C for 5 h. Each filter was rinsed in bi-distilled water (to eliminate the residual ceramic paste) and, then, dried in an oven at 100 °C for about 30 min.

The so prepared filters were coated with ceria. To this end, a dip coating procedure was employed starting from a colloidal suspension (NYACOL, CeO_2 (AC)) consisting of nano-sized ceria particles dispersed in a solution of acetic acid (particle size: 10–20 nm). The filter was dipped for 5 min in 50 ml of colloidal suspension and, then, rotated and dipped for further 5 min. After dipping, the filter was vigorously shaken to eliminate the excess material, dried at 120 °C for 40 min and, then, calcined at 450 °C for 2 h. The cycle of dipping, shaking, drying and calcination was repeated three times to achieve the desired target (~1 g).

After the catalyst-coating, the filters were loaded with soot. To this end, the technique described in van Setten et al. [20] was adopted. In particular, the filter was dipped in a suspension of soot (1 g - Degussa Printex U) in heptane (100 ml - Sigma–Aldrich). The duration time of the dipping phase and the number of repetitions of the whole procedure were varied to vary the soot load (and, thus, the catalyst/soot ratio). After dipping, the filter was vigorously shaken and, then, dried for 1 h at room temperature (to allow the heptane evaporation).

Fig. 1 shows the monoliths after the steps of cutting, plugging, catalyst-coating and soot-loading (along with the original IBIDEN filter).

The step of soot-loading and the step of catalyst-coating were skipped to prepare catalyst-coated filters (for characterization) and soot-loaded filters (for characterization and thermal regeneration test), respectively. The catalyst/soot ratio was varied from 0 to 98 w/w.

2.2. Filter characterization

Filter samples (filter as it is, catalyst-coated filter, soot-loaded filter and filters with two different CeO_2/soot ratios) were characterized.

The pore size distribution (PSD) in the region of macro-pores was evaluated using a Micromeritics Autopore IV by the Hg intrusion porosimetry technique. Specific surface area measurements and micro- and meso-pore analysis were performed with a Quantachrome Autosorb 1-C by N_2 adsorption at 77 K after degassing the samples for 2 h at 150 °C. The specific surface area was evaluated through the BET method, whereas the PSD of micro- and meso-pores was evaluated through the BJH method.
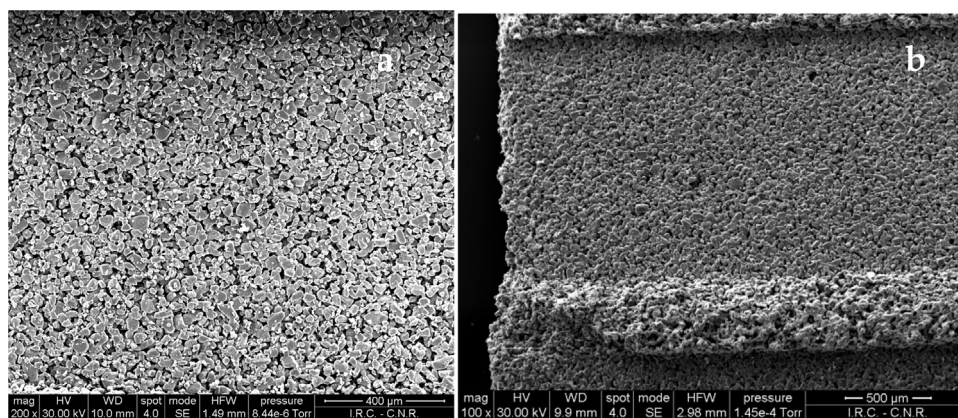
Fig. 4. SEM images of the channel surface: original filter (a); CeO_2-coated filter (b).
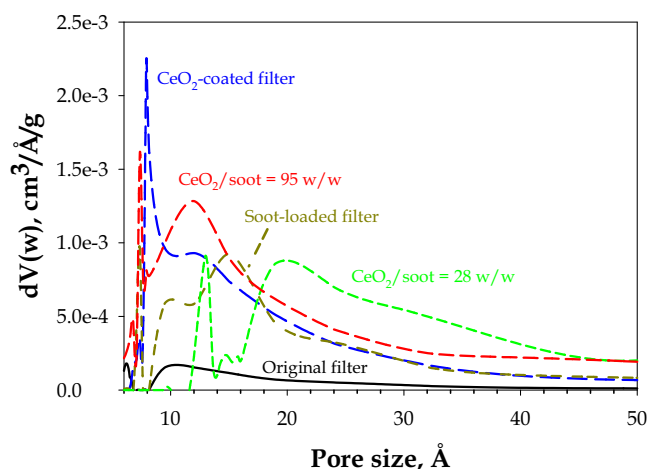

Fig. 5. Pore size distribution (PSD) in the region of micro- and meso-pores for original filter, soot-loaded filter, CeO_2-coated filter, and two filters with different CeO_2/soot ratios.

The internal morphology of filter channels was observed using a FEI Inspect Scanning Electron Microscope (SEM) equipped with an energy dispersive X-ray (EDX) probe for the elemental mapping.

2.3. Apparatus for regeneration tests

Temperature programmed soot combustion tests were performed in a lab-scale rig. The filter was placed in a tubular quartz reactor (diameter = 2.54 cm). A mullite foam (same cross-section as the filter; length = 0.5 cm) was placed upstream the inlet section of the filter to ensure a uniform distribution of the gas flow. Both filter and foam were wrapped in a ceramic wool tape.

The reactor was placed in a tubular electric oven (LENTON Ltd. mod. PTF 12/38/500; length = 60 cm; length of the isothermal zone ~5 cm) equipped with a PID controller to perform regeneration tests at controlled heating rate. The filter was pre-heated at 250 °C in nitrogen stream (0.5 l(STP)/h) and, then, heated up to 700 °C at a rate of 5 °C/min.

Brooks 5850S mass flow controllers for N_2 and O_2 were used to set up flow rate and composition of the feed to the reactor. In particular, the total flow rate was set equal to 47 l(STP)/h, and the concentration of O_2 in N_2 equal to 15 vol.%.

The gas mixture exiting the reactor entered an analysis system including a Fisher-Rosemount NGA2000 analyzer for simultaneous analysis of CO and CO_2 by IR detectors, and O_2 by a paramagnetic detector. The filter was weighted before and after each regeneration test to verify the carbon balance through the comparison between the amount of disappeared/consumed soot and the amount of produced CO and CO_2. The carbon balance was closed with an error of ±10%.

A four-way ball-valve was used to by-pass the reactor, thus enabling the measurement of the feed composition by using the same analyzer. Data were continuously recorded on a PC through a data acquisition system developed in LabView environment.

The filter temperature was measured by the insertion of thermocouples at the entrance and exit of the central channel. An electronic pressure transducer measured the pressure drop across the filter.

Regeneration tests were performed by varying the catalyst/soot ratio (from 0 - thermal regeneration - to 98 w/w). In all tests, the two upstream and downstream filter temperatures were substantially the same and followed the expected heating ramp. Furthermore, all tests were highly repeatable. As an example of such repeatability, Fig. 2 shows the CO_2 concentration-filter temperature profiles as measured during two independent regeneration tests carried out on two filters with catalyst/soot ratio equal to 45 w/w. The two filters were independently prepared following the same procedure (i.e., the four steps of cutting, plugging, catalyst-coating and soot-loading of Fig. 1).

3. Results and discussion

3.1. Filter characterization

Macro-pores of the original filter, evaluated by Hg porosimetry, account for 46% porosity, in good agreement with the value provided by the supplier (42%).

Fig. 3 shows the pore size distribution (PSD) in the region of macro-pores for four samples: original filter, CeO_2-coated filter and two filters with different CeO_2/soot ratios.

The original filter exhibits a quite narrow pore distribution peaked at 11000–12000 nm, resulting from SiC inter-particle spaces. After the catalyst-coating, the pore distribution slightly changes, showing a peak at about 10000 nm. This suggests that the deposition of ceria nanoparticles inside the filter walls results in a limited occlusion of macro-pores, thus preserving the filtering properties. On the contrary, the soot loading results in a progressive reduction of the fraction of large macro-pores, along with the appearance of smaller pores (<5000 nm). This means that an occlusion of large macro-pores occurs.

The SEM images of Fig. 4 show the channel surface of the original filter (a) and that of the CeO_2-coated filter (b).

The typical granular structure of the SiC filter (i.e., the network of SiC particles) is still preserved after the catalyst deposition, thus confirming the results obtained by Hg porosimetry. The ceria
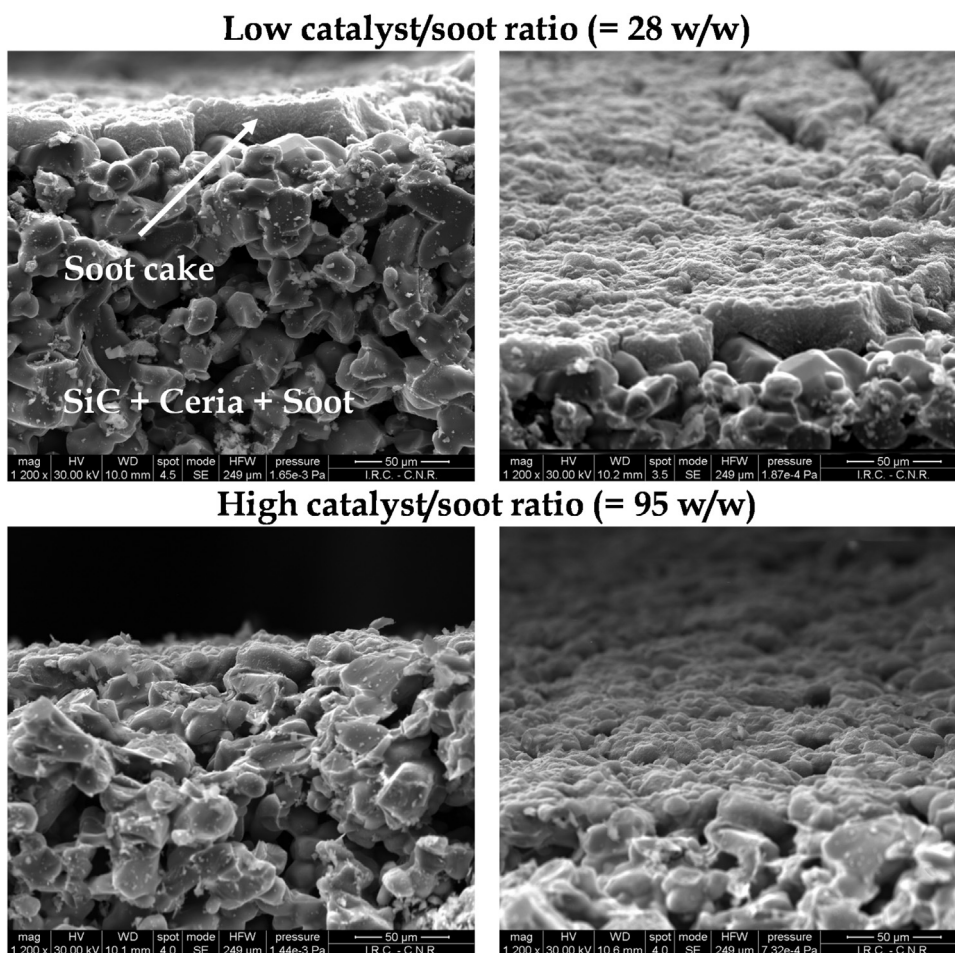
Low catalyst/soot ratio (= 28 w/w)

High catalyst/soot ratio (= 95 w/w)

Fig. 6. SEM images of cross section of filter channel for two samples with low (top) and high (bottom) CeO$_2$/soot ratio. In the left pictures, the samples are perpendicular to the radiation; in the right pictures, the tilt angle of radiation is higher than 90 degrees.
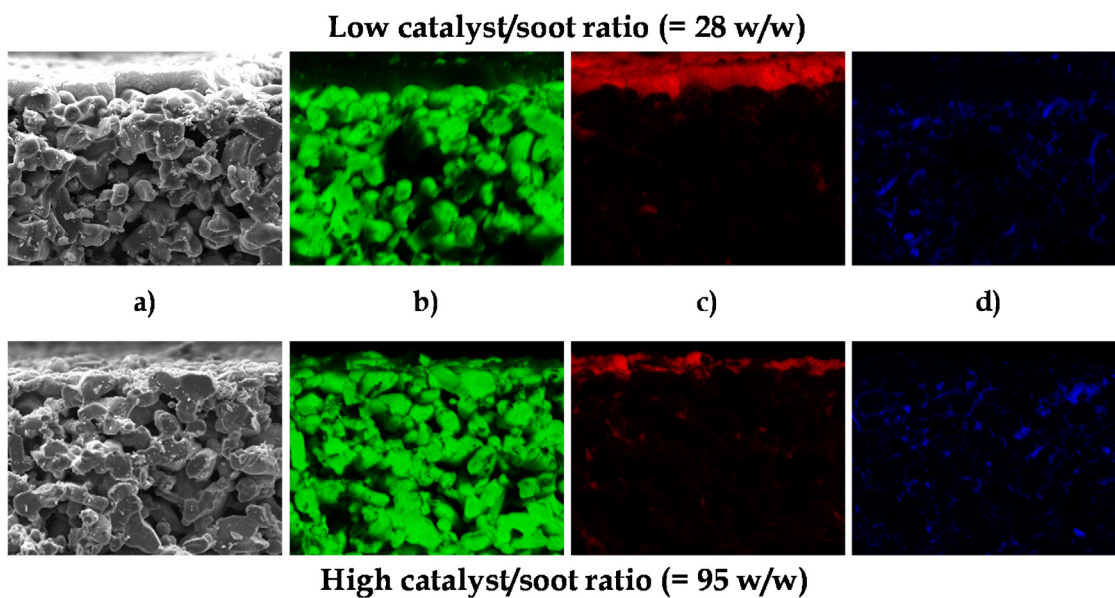
Low catalyst/soot ratio (= 28 w/w)

High catalyst/soot ratio (= 95 w/w)

Fig. 7. EDX mapping of cross section of filter channel for two samples with low (top) and high (bottom) CeO$_2$/soot ratio: (a) SEM images and distribution of (b) Si, (c) C, (d) Ce.

nanoparticles penetrate into the macro-pores avoiding the accumulation of a catalyst layer on top of the filter wall.

In Table 1, the specific surface area and the pore volume (i.e., the volume of micro- and meso-pores) are reported for the original filter, the soot-loaded filter, the CeO$_2$-coated filter and the two filters

Table 1

Specific surface area and pore volume (i.e., volume of micro- and meso-pores) for original filter, soot-loaded filter, CeO_2-coated filter, and two filters with different CeO_2/soot ratios.

Sample	Specific surface area (m²/g)	Pore volume (cm³/g)
Original filter	3	0.0033
Soot-loaded filter	10	0.017
CeO_2-coated filter	16	0.022
Filter with CeO_2/soot ratio = 95 w/w	22	0.033
Filter with CeO_2/soot ratio = 28 w/w	24	0.034

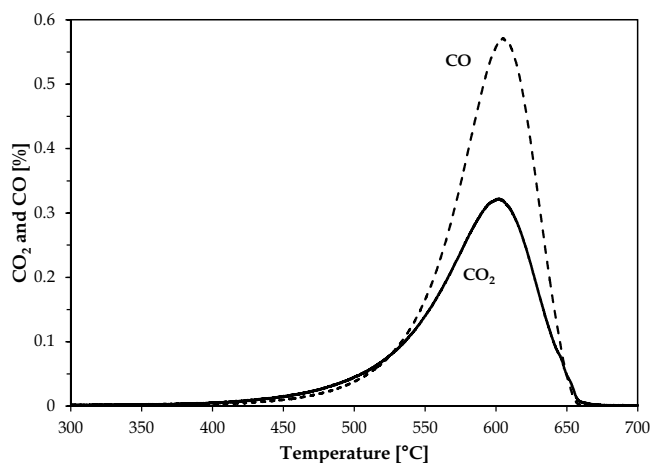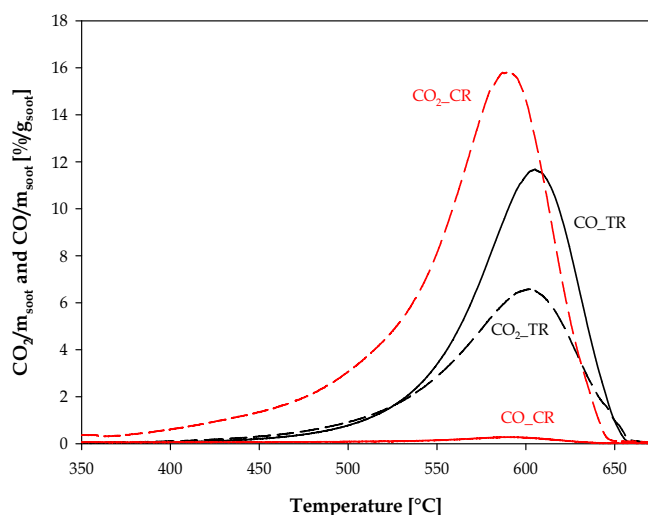**Fig. 8.** CO_2 and CO concentration as a function of the filter temperature: thermal regeneration.

Fig. 9. Normalized CO_2 (dashed lines) and CO (solid lines) concentration as a function of the filter temperature: thermal regeneration (TR) and catalytic regeneration (CR; catalyst/soot ratio = 20 w/w).
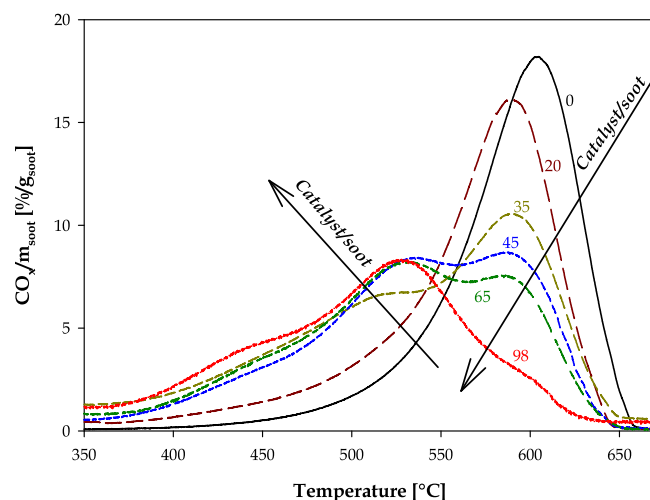

Fig. 10. Normalized CO_x concentration as a function of the filter temperature for different catalyst/soot ratios (w/w).

and, thus, micro- and meso-pores increase as well. However, the combined effect of ceria and soot is less than additive.

The PSD in the region of micro- and meso-pores shown in Fig. 5 confirms the above considerations.

The CeO_2 coating results in a large increase of pores in the range 10–40 Å, along with a more pronounced micro-porosity peaked at around 7 Å. The soot-loaded filter exhibits pores in the same range as the catalyst-coated filter, even if more centered at higher size.

The surface area and the pore volume both increase when ceria and soot are simultaneously present on the filter providing very similar values (Table 1). Nevertheless, the PSD is different depending on the CeO_2/soot ratio. At high CeO_2/soot ratio (95 w/w), the average pore size is centered at lower values, whilst at low CeO_2/soot ratio (28 w/w), there is a larger contribution of pores with size higher than 20 Å.

It is worth highlighting that the data related to the changes in exposed surface area and porosity, when the filter is first coated with catalytic material and then loaded with soot, are likely to be very useful in modelling the operation of this technology.

In Fig. 6, the SEM images of the cross section of the filter channel are shown for the two samples with low (top) and high (bottom) CeO_2/soot ratio. In the left pictures, the samples are perpendicular to the radiation; in the right pictures, the tilt angle of radiation is higher than 90 degrees to better show the morphology of the soot deposition onto the channel surface. These images, along with the results of the EDX elemental mapping shown in Fig. 7, are useful to describe the interaction occurring among soot, catalyst and SiC.

At low CeO_2/soot ratio (28 w/w), i.e., in the presence of high amount of soot, the typical soot cake (thickness of around 15–20 μm) appears on the surface of the filter wall, in addition to a small fraction of soot that deeply penetrates into the filter macro-pores coming in close touch with highly dispersed ceria. This is also confirmed by the EDX elemental distribution of Fig. 7 (top). Yapaulo et al. [17] found the same kind of soot distribution in a real DPF: some soot deeply penetrates into the wall, whereas the majority of soot stays very close to the wall surface.

It is worth noting that the soot-ceria contact conditions established inside the filter wall look like those reported by Bensaid et al. [12] in the case of the fibrous ceria morphology, i.e., a network of fibers which surround the soot particles, thus maximizing the number of contact points. On the other hand, the size of the ceria aggregates inside the filter wall is below 20 μm and that of the penetrated soot particles even smaller, condition that can virtually promote a good soot-catalyst contact. Indeed, Iojoiu et al. [21]

with different CeO_2/soot ratios. Fig. 5 shows the PSD in the region of micro- and meso-pores for the same filter samples.

The specific surface area of the original filter is very low as well as the pore volume. The deposition of CeO_2 and soot leads to an increase of both surface area and pore volume. This can be linked to the decrease of macro-pore size and (especially in the case of soot deposition) volume, which is counterbalanced by the increase of micro- and meso-pores, and also to the contribution of micro- and meso-pores intrinsically present in both ceria and soot. In going from the original filter to the filter with CeO_2/soot ratio equal to 28 w/w, the overall amount of ceria + soot increases
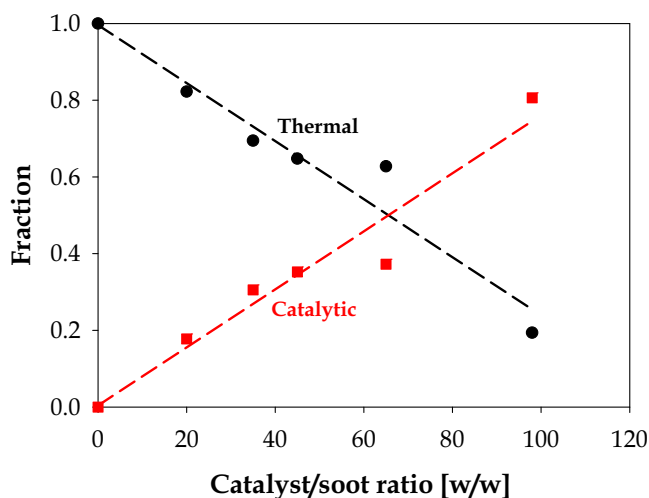
Fig. 11. Fraction of catalytically converted soot (along with the complementary fraction of thermally converted soot) as a function of the catalyst/soot ratio.
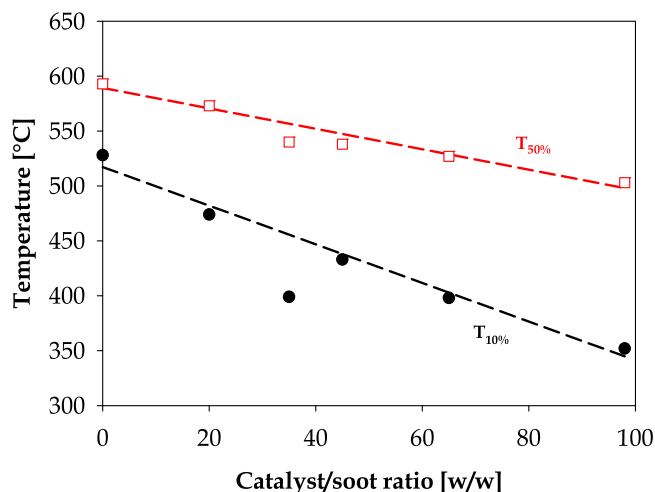

Fig. 12. Temperature at which 10% ($T_{10\%}$) and 50% ($T_{50\%}$) of the initial soot is converted as a function of the catalyst/soot ratio.

reported that, when applying "highly tight" contact conditions to powder samples (i.e., when ball milling ceria and soot), the soot-catalyst aggregates show a bi-modal distribution of the particle sizes with the main peak centered at about 15 μm.

At high CeO_2/soot ratio (95 w/w), the cake layer becomes very thin, although the morphology of the soot deposition onto the channel surface seems to be very similar to that of the other sample. The EDX results of Fig. 7 (bottom) confirm the very small cake thickness, along with the incorporation of CeO_2 and soot inside the filter macro-pores. Thus, the high CeO_2/soot ratio assures a better soot-catalyst contact, avoiding a large accumulation of soot onto the filter wall in the form of cake layer, which is substantially segregated from the catalyst.

Figs. 6 and 7 allow a clear distinction between two filter zones: an internal zone, which is the catalytic porous wall of the filter, and an external zone, which is the cake layer. At low CeO_2/soot ratio, the external zone is well distinct from the internal one, whereas at high CeO_2/soot ratio, it is quite negligible, the soot particles being almost totally included inside the filter macro-pores. In order to quantify the role played by both external and internal zones in affecting the regeneration performance, temperature programmed combustion tests were performed on filters with catalyst/soot ratio varying from 0 (thermal regeneration) to 98 w/w.

3.2. Regeneration tests

3.2.1. Thermal regeneration

Fig. 8 shows the results obtained from the thermal regeneration test, in terms of CO_2 and CO concentration as a function of the filter temperature.

Both profiles exhibit a peak at around 600 °C. The ratio between the areas of the two profiles provided a selectivity to CO_2 of about 40%. Thus, during thermal regeneration, most of the soot is converted into CO (rather than into CO_2). Rico Pérez and Bueno-López [19] found a similar value of selectivity to CO_2 (∼50%) in their tests of thermal regeneration of DPFs.

3.2.2. Comparison between thermal and catalytic regeneration

In Fig. 9, the results of Fig. 8 (thermal regeneration, TR) are plotted in comparison with the results obtained from a catalytic regeneration (CR) test performed on a filter having catalyst/soot ratio equal to 20 w/w.

It is worth saying that all the results were normalized with respect to the mass of soot loaded into the filter (for each test), m_{soot}. Thus, both profiles of CO_2 and CO as well as their underlying areas are directly comparable.

When moving from thermal to catalytic regeneration, the concentration profiles shift towards slightly lower temperatures (the shift is of around 10 °C). Indeed, the most apparent effect of the catalyst presence is on the selectivity to CO_2, which increases from ∼40% (TR) to ∼98% (CR). This means that the catalyst activates CO oxidation. Similar values of selectivity to CO_2 (∼95%) were found during regeneration tests of DPFs loaded with an optimized ceria-praseodymia active phase [19].

The results of the filter characterization have shown that, at low CeO_2/soot ratio (28 w/w), in addition to the soot particles penetrated into the catalytic filter wall (internal zone), where a good solid–solid contact is established, a rather thick soot cake (external zone) is formed, which is segregated from the catalyst. Thus, the slight shift of the concentration profiles towards lower temperatures can be attributed to the catalytic conversion of a small fraction of the overall soot (i.e., the soot inside the filter wall), whereas most of the soot (i.e., the cake layer) is still converted via the non-catalytic (thermal) path. In other words, the soot-catalyst contact is too weak and, as found in the experiments by Rico Pérez and Bueno-López [19], the process of catalytic regeneration is somewhat hindered. However, in the presence of catalyst, most of CO, which is thermally produced, is converted into CO_2, being CO oxidation independent of the soot-catalyst contact.

3.2.3. Effect of the catalyst/soot ratio

Fig. 10 shows the plots of normalized CO_x (=CO_2 + CO) concentration versus temperature for catalyst/soot ratio varying from 0 (thermal regeneration) to 98 w/w. For the catalytic tests, CO_x is substantially CO_2 - this especially true for catalyst/soot ratio ≥35 w/w, when the selectivity to CO_2 overcomes 99%.

Starting from catalyst/soot ratio equal to 35 w/w, a double-peaked shape appears. The higher temperature peak is still centered at ∼590 °C (as the peak observed at catalyst/soot ratio equal to 20 w/w), whereas the lower temperature peak is centered at ∼520 °C and exhibits a shoulder at ∼450 °C. The lower temperature contribution becomes almost the unique one for catalyst/soot ratio equal to 98 w/w. On the other hand, the results of the filter characterization have shown that, at high CeO_2/soot ratio (95 w/w), a very thin cake layer is formed and most of the soot particles deeply penetrate into the macro-pores of the filter wall, where the catalyst is highly dispersed, resulting in a very effective solid–solid contact. Thus, the lower temperature peak can be reasonably attributed to catalytic soot oxidation.
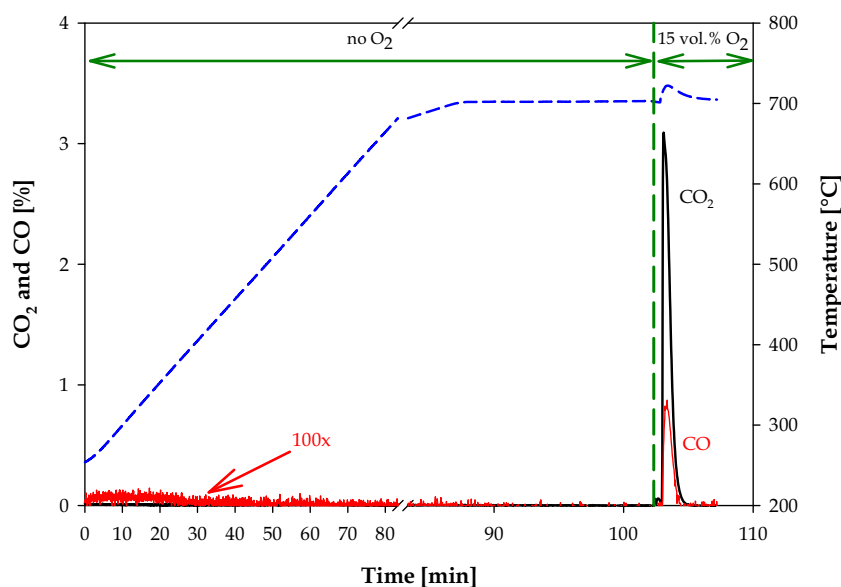
Fig. 13. CO_2 and CO concentration and filter temperature versus time: catalytic regeneration in the absence (and presence) of gas-phase O_2 (catalyst/soot ratio equal to 125 w/w).

Fig. 10 shows that better regeneration performance is found with increasing catalyst/soot ratio. This is a direct consequence of the decreased cake thickness and, thus, of the decreased role played by the external zone with respect to that played by the internal one (catalytic filter wall). Indeed, as the cake thickness is decreased, overall better conditions of soot-catalyst contact are established, which allow to move from a catalyst-assisted thermal regeneration mode (catalyst/soot ratio = 20; 35; 45; 65 w/w) to an almost purely catalytic regeneration mode (catalyst/soot ratio = 98 w/w).

In the case of the catalyst-assisted thermal regeneration mode, a double-step oxidation mechanism takes place: (1) internal zone − catalytic soot oxidation to CO_2; (2) external zone - thermal oxidation of the soot cake mainly to CO, which is catalytically oxidized to CO_2 at higher temperature. In the case of the almost purely catalytic regeneration mode, the cake layer is almost undetectable and soot oxidation substantially occurs according to step (1) (step (2) plays a minor role).

In order to quantitatively assess the fraction of catalytically converted soot (with respect to the overall amount of combusted soot), the deconvolution of the concentration curves of Fig. 10 into the two (catalytic and thermal) contributions was performed. To this end, the Fityk software (free version 0.9.1) was used [22].

Fig. 11 shows the fraction of catalytically converted soot (along with the complementary fraction of thermally converted soot) as a function of the catalyst/soot ratio.

The fraction of catalytically converted soot increases roughly linearly with increasing catalyst/soot ratio. In particular, for the ratios corresponding to the catalyst-assisted thermal regeneration mode (20; 35; 45; 65 w/w), the catalytic fraction is always lower than 0.5. Conversely, for the almost purely catalytic regeneration mode (98 w/w), it is equal to around 0.8.

To quantify the improvement in terms of regeneration performance, the temperatures at which 10% and 50% of the initial soot is converted ($T_{10\%}$ and $T_{50\%}$, respectively) were extracted from the concentration curves of Fig. 10. Fig. 12 shows the plots of $T_{10\%}$ (onset temperature) and $T_{50\%}$ (half-conversion temperature) versus the catalyst/soot ratio.

Both temperatures decrease with the catalyst/soot ratio. In particular, when moving from thermal regeneration (catalyst/soot ratio = 0) to almost purely catalytic regeneration (catalyst/soot ratio = 98 w/w), $T_{10\%}$ decreases from ∼525 °C to ∼350 °C. Indeed,

the onset temperature is more sensitive than the half-conversion temperature to variations in the catalyst/soot ratio and, thus, to variations in the soot-catalyst contact conditions. This trend has also been found in catalytic combustion experiments with a ceria catalyst mixed in "loose" (with a spatula) and "tight" (in a mortar) contact with soot [11].

Fig. 13 shows the results of a catalytic regeneration test carried out in the absence of gas-phase O_2 and under conditions of good soot-catalyst contact (i.e., catalyst/soot ratio equal to 125 w/w). In the figure, the concentrations of CO_2 and CO are plotted versus time along with the filter temperature.

In the absence of gas-phase O_2, no CO_x evolution was detected. Thus, O_2 was fed, leading to a rapid CO_x evolution. These results highlight the key role of the gas-phase O_2 in ceria-catalyzed soot combustion.

4. Conclusions

The effect of the soot-catalyst contact on the regeneration performance of a diesel particulate filter (DPF) wash-coated with highly dispersed nano-metric ceria particles was investigated by varying the soot load and, thus, the catalyst/soot ratio.

Two different types of soot distribution have been found:

1) at high catalyst/soot ratio (∼100 w/w), the soot particles deeply penetrate into the macro-pores of the filter walls (internal zone of the filter) coming in close touch with ceria;
2) at low catalyst/soot ratio (∼20 w/w), in addition to the soot particles trapped inside the macro-pores, a thick soot cake layer accumulates on top of the catalytic filter walls (external zone of the filter).

In going from condition (1) to condition (2), a transition occurs from an almost purely catalytic regeneration mode (with a large fraction of soot - around 80% - burned via catalytic path) to a catalyst-assisted thermal regeneration mode (with around 80% of soot burned via thermal path). This is a direct consequence of the increased cake thickness and, thus, of the increased role played by the external zone with respect to that played by the internal one. Indeed, condition (1) corresponds to effective soot-catalyst contact: the ceria catalyst catalyzes direct combustion of soot,

resulting in good regeneration performance (e.g., temperature at which 10% of the initial soot is converted, $T_{10\%}$, equal to around 350 °C). Conversely, condition (2) corresponds to poor soot-catalyst contact and, thus, much worse regeneration performance (e.g., $T_{10\%}$ ~475 °C): the ceria catalyst predominantly catalyzes oxidation of CO, which is the product of incomplete (thermal) oxidation of soot.

The results obtained in this work highlight the importance of strategies that avoid or minimize the segregation between the cake layer and the catalytic wall of the filter to operate catalyst-coated DPFs in an effective manner. Indeed, in spite of the considerable efforts made in the design of ceria-based soot combustion catalysts at laboratory [3,10,11], the main challenge still remains to increase the soot-ceria contact surface greatly on the filter.

Acknowledgements

References

[1] G.C. Koltsakis, O.A. Haralampous, Z.C. Samaras, L. Kraemer, F. Heimlich, K. Behnk, SAE Technical Paper 2007-01-1127 (2007).
[2] D. Fino, V. Specchia, Powder Technol. 180 (2008) 64–73.
[3] D. Fino, S. Bensaid, M. Piumetti, N. Russo, Appl. Catal. A Gen. 509 (2016) 75–96.
[4] P.A. Kumar, M.D. Tanwar, S. Bensaid, N. Russo, D. Fino, Chem. Eng. J. 207-208 (2012) 258–266.
[5] B. Guan, R. Zhan, H. Lin, Z. Huang, J. Environ. Manag. 154 (2015) 225–258.
[6] T. Maunula, P. Matilainen, M. Louhelainen, P. Juvonen, T. Kinnunen, SAE Technical Paper 2007-01-0041 (2007).
[7] B.W.L. Southward, S. Basso, M. Pfeifer, SAE Technical Paper 2010-01-0558 (2010).
[8] B.A.A.L. van Setten, J.M. Schouten, M. Makkee, J.A. Moulijn, Appl. Catal. B Environ. 28 (2000) 253–257.
[9] K. Hinot, H. Burtscher, A.P. Weber, G. Kasper, Appl. Catal. B Environ. 71 (2007) 271–278.
[10] E. Aneggi, C. de Leitenburg, A. Trovarelli, Catalysis by Ceria and Related Materials, in: A. Trovarelli, P. Fornasiero (Eds.), second ed., Imperial College Press, London, 2013, pp. 565–621.
[11] A. Bueno-López, Appl. Catal. B Environ. 146 (2014) 1–11.
[12] S. Bensaid, N. Russo, D. Fino, Catal. Today 216 (2013) 57–63.
[13] E. Aneggi, D. Wiater, C. De Leitenburg, J. Llorca, A. Trovarelli, ACS Catal. 4 (2014) 172–181.
[14] P. Miceli, S. Bensaid, N. Russo, D. Fino, Nanoscale Res. Lett. 9 (2014) 254.
[15] P. Miceli, S. Bensaid, N. Russo, D. Fino, Chem. Eng. J. 278 (2015) 190–198.
[16] M. Piumetti, S. Bensaid, N. Russo, D. Fino, Appl. Catal. B Environ. 165 (2015) 742–751.
[17] R.A. Yapaulo, E. Wirojsakunchai, T. Orita, D.E. Foster, M. Akard, L.R. Walker, M.J. Lance, Int. J. Engine Res. 10 (2009) 287–304.
[18] V. Di Sarli, A. Di Benedetto, Chem. Eng. Sci. 137 (2015) 69–78.
[19] V. Rico Pérez, A. Bueno-López, Chem. Eng. J. 279 (2015) 79–85.
[20] B.A.A.L. van Setten, P. Russo, S.J. Jelles, M. Makkee, P. Ciambelli, J.A. Moulijn, React. Kinet. Catal. Lett. 67 (1999) 3–7.
[21] E.E. Iojoiu, B. Bassou, N. Guilhaume, D. Farrusseng, A. Desmartin-Chomel, K. Lombaert, D. Bianchi, C. Mirodatos, Catal. Today 137 (2008) 103–109.
[22] M. Wojdyr, J. Appl. Cryst. 43 (2010) 1126–1128.